Location Estimation Accuracy of Augmented Arrays for Millimeter-Wave FMCW-MIMO Radar

Koichi Ichige†, Ryo Saito†, Tomoya Sugiyama†, Nobuya Arakawa‡, Katsuhisa Kashiwagi‡, Atsuyuki Yuasa‡

† Dept. Electrical & Computer Eng., Yokohama Nat'l Univ., Yokohama-shi, Kanagawa 240-8501, Japan.
‡ Murata Manufacturing Co., Ltd., Nagaokakyo-shi, Kyoto 617-8555, Japan.

2019 International Radar Conference (RADAR) 978-1-7281-2660-9/20/$31.00 ©2020 IEEE 10.1109/RADAR41533.2019.171258

***Abstract*—In this paper, we examine the performance of location estimation with various estimation methods for the millimeter-wave frequency modulated continuous wave (FMCW)-MIMO radar. We do not aim for any novel estimation method but evaluate the resolution of angle and distance estimation in great detail through simulation and experiments. We found through our simulation and experimental results that Khatri-Rao (KR) product extension is often effective for the radar and can well improve the accuracy of location estimation. We clarify the properties and drawbacks of the location estimation methods through our simulation and experimental results.**

***Index Terms*—FMCW-MIMO radar, location estimation, direction of arrival estimation**

I. Introduction

There has been a lot of development on automotive radar technology in the last decade toward self-driving cars [1] and advanced driver-assistance systems (ADAS) [2]. We can detect objects around a car by analyzing received signals or images measured by sensors like the millimeter (MM)-wave radar [3] or light detection and ranging (LiDAR). Indeed, the MM-wave radar is very attractive as a high resolution sensor that is not affected much by bad weather or darkness, and it is expected to be used as a sensor not only for automotive radars but for various kinds of applications [4],[5]. The locations of objects can be estimated by using any direction of arrival (DOA) estimation method with an array antenna [6] or by combining DOA and time of flight (TOF) information [7]–[8].

One may use the multiple-input multiple-output (MIMO) system in order to improve the estimation accuracy of the MM-wave radar. The MIMO radar can virtually increase the number of receiver array elements by using multiple transmitters, and it enables higher resolution DOA estimation than the classical single-input multiple-output (SIMO) radar [9]. For DOA estimation methods, we evaluate the classical beamformer (BF) based on the spatial fast Fourier transform (FFT), the multiple signal classification (MUSIC) [10] method, and the estimation of signal parameters via rotational invariance techniques (ESPRIT) [11] method based on the eigendecomposition of the covariance matrix of array input. Also, it is well-known [6] that eigen-based methods like MUSIC or ESPRIT can separate multiple signal sources more accurately than the BF method. Moreover, spatial smoothing preprocessing (SSP) [12] is combined with MUSIC or ESPRIT when estimating the DOAs of multiple coherent or highly correlated sources.

To increase the resolution in DOA estimation, Khatri-Rao (KR) product extension [13] also combined with MUSIC or ESPRIT has already been investigated [9]. With these methods, we can virtually increase the number of array elements as well as data samples and can enhance the degree of freedom (DOF), DOA, and distance estimation accuracy. Moreover, non-uniform array configurations like the nested array [14] have also been studied and attracted attention. This array can virtually create a larger array aperture with KR product extension. The nested array can create a higher number of virtual array elements than the uniform linear array (ULA) through the application of KR product extension, and, therefore, a higher angular resolution can be achieved. However, KR product extension causes large errors when estimating two or more locations due to the correlation between two incident waves.

In this paper, we examine the performance of location estimation with various estimation methods for the MM-wave frequency modulated continuous wave (FMCW)-MIMO radar. We do not aim for any novel estimation method but evaluate the resolution of angle and distance estimation in great detail through simulation and experiments. As mentioned above, we evaluate representative methods like the BF, MUSIC and ESPRIT methods, with or without SSP and/or KR product extension.

II. Preliminaries

In this section, we briefly review the signal model in the FMCW-MIMO radar, array extension, and DOA estimation algorithms.

A. Signal model

Consider a MIMO radar system with K_T transmitter and K_R receiver antenna elements and L reflectors (objects to be specified) in a far field under an additive white Gaussian noise (AWGN) environment. The received chirp (FMCW) signals are modified into beat signals by calculating the difference between the transmitted and received chirp signals, applying FFT, and extracting only large (beat) frequency components.

The $K_T \times K_R$ MIMO system is equivalent to a virtual $K = K_T \cdot K_R$ SIMO system and is often replaced with it for simplification; the array input signal vector $\boldsymbol{x}(t)$ of the SIMO system is written as

$$\boldsymbol{x}(t) = \boldsymbol{A}\boldsymbol{s}(t) + \boldsymbol{n}(t), \tag{1}$$

978-1-7281-2660-9/19/$31.00 ©2019 IEEE

where the matrix $\boldsymbol{A}$ denotes an array steering matrix whose column vectors are steering vectors indicating the phase difference information between array elements, and $\boldsymbol{s}(t)$ and $\boldsymbol{n}(t)$ respectively denote incident (beat) signal and noise vectors. DOAs are estimated by using the cross-correlation matrix $\boldsymbol{R}_{xx}$ of the signal vectors, which is defined by

$$\boldsymbol{R}_{xx} = \boldsymbol{A}\boldsymbol{S}\boldsymbol{A}^H + \sigma^2\boldsymbol{I} \simeq \sum_{t=1}^{N} \boldsymbol{x}(t)\boldsymbol{x}^H(t), \tag{2}$$

where N denotes the number of temporal snapshots. The matrix $\boldsymbol{S}$ is the wave-source correlation matrix where incident wave information is stored in diagonal and off-diagonal elements. Note that the cross-correlation matrix in the radar system is calculated from the complex spectrum of the amplitude peak frequency [7], i.e.,

$$\boldsymbol{R}_{xx}(f_m) = \boldsymbol{X}(f_m)\boldsymbol{X}^H(f_m), \tag{3}$$

where $\boldsymbol{X}$ and f_m respectively denote the beat signal amplitude and peak frequency of the magnitude spectrum.

B. KR product extension

Vectorizing the correlation matrix R_{xx} in (2), we have

$$\begin{aligned} \boldsymbol{z} &= \mathrm{vec}(\boldsymbol{R}_{\mathrm{xx}}) \\ &= \mathrm{vec}(\boldsymbol{A}\boldsymbol{S}\boldsymbol{A}^H) + \mathrm{vec}(\sigma^2\boldsymbol{I}) \\ &= (\boldsymbol{A} \odot \boldsymbol{A})\boldsymbol{p} + \mathrm{vec}(\sigma^2\boldsymbol{I}), \end{aligned} \tag{4}$$

where $\odot$ is an operator representing the KR product, and vec$(\cdot)$ is a vectorizing operator. Also, $\boldsymbol{p}$ is a vector composed of diagonal elements of $\boldsymbol{S}$ and represents the power of a signal. $(\boldsymbol{A} \odot \boldsymbol{A})$ is regarded as a new direction matrix, $\boldsymbol{A}, \boldsymbol{p}$ as a signal vector, and $\boldsymbol{z}$ can be regarded as a new received signal vector.

Since the number of rows of a received signal is changed from K to K^2, the number of antenna elements, that is, the aperture, increases. When the position vector of the antenna array is $\boldsymbol{d}_k, (k = 0, 1, \cdots, K-1)$, the position of the extended virtual array obtained by the received signal vector $\boldsymbol{z}$ is $\boldsymbol{d}_i - \boldsymbol{d}_j, (i, j = 0, 1, \cdots, K-1)$. The aperture length in the actual KR-product-extended received signal is determined by how many different values $d_i - d_j$ there are, which is the difference in antenna element locations. In general, the entries of $(\boldsymbol{A} \odot \boldsymbol{A})$ may contain duplications, so we consider a vector without duplicate components to be $\boldsymbol{z}_1 = \boldsymbol{A}_1\boldsymbol{p} + \sigma^2\boldsymbol{e}$, where $\boldsymbol{A}_1$ is a matrix obtained by removing duplicated components of $(\boldsymbol{A} \odot \boldsymbol{A})$, $\boldsymbol{e}$ is a vector of only one component whose value is 1, and all other components are zeros. Then, DOAs can be estimated by calculating the correlation matrix $\boldsymbol{R}_{zz}$ by using this vector $\boldsymbol{z}_1$.

C. DOA estimation algorithms

In this section, we briefly review the location estimation methods used in the simulation and experiments. Hereinafter, the modified versions of the BF and MUSIC methods proposed in [9] are called "2D-BF" and "2D-MUSIC" methods, respectively.

As a location estimation method that performs both distance and DOA estimation at the same time, we briefly review the 2D-BF method proposed in [9]. As an example, we consider a case of a K-element ULA with a number of sample snapshots N. The received signal vector x_{2d} obtained by rearranging the received signals of the respective received elements in the order of sampling points is expressed by the following equation.

$$\boldsymbol{x}_{2d} = [\boldsymbol{x}(1), \cdots, \boldsymbol{x}(N)]^T, \tag{5}$$

$$\boldsymbol{x}(n) = [\boldsymbol{x}_1(n), \cdots, \boldsymbol{x}_k(n), \cdots, \boldsymbol{x}_K(n)], \tag{6}$$

where $\boldsymbol{x}_k(n)$ represents the received data of the n-th sampling point of the k-th receiving element. The received signal vector $\boldsymbol{x}_{2d}$ has KN elements. Next, the correlation matrix $\boldsymbol{R}_{xx}$ is generated from the received signal vector $\boldsymbol{x}_{2d}$ as $\boldsymbol{R}_{xx} = E[\boldsymbol{x}_{2d}\boldsymbol{x}_{2d}^H]$. By multiplying this correlation matrix by a mode vector $\boldsymbol{a}(\theta, \tau)$, we can calculate the distance and angle spectrum $\boldsymbol{P}_{BF}(\theta, \tau)$. The spectrum calculation formula is

$$\boldsymbol{P}_{2D-BF}(\theta, \tau) = \frac{\boldsymbol{a}^H(\theta, \tau)\boldsymbol{R}_{xx}\boldsymbol{a}(\theta, \tau)}{\boldsymbol{a}^H(\theta, \tau)\boldsymbol{a}(\theta, \tau)}, \tag{7}$$

$$\boldsymbol{a}(\theta, \tau) = \boldsymbol{a}_1(\tau) \otimes \boldsymbol{a}_2(\theta), \tag{8}$$

$$\boldsymbol{a}_1(\tau) = \left[1, e^{j\mu\tau\Delta t}, \cdots, e^{j\mu(N-1)\tau\Delta t}\right]^T, \tag{9}$$

$$\boldsymbol{a}_2(\theta) = \left[1, e^{j\frac{2\pi}{\lambda}d\sin\theta}, \cdots, e^{j\frac{2\pi}{\lambda}(K-1)d\sin\theta}\right]^T, \tag{10}$$

$$\mu = \frac{2\pi B_w}{T_m}, \tag{11}$$

where $\boldsymbol{a}_1(\tau)$ and $\boldsymbol{a}_2(\theta)$ are steering vectors having the information of time and angle, respectively. Then, the Kronecker product of these vectors $\boldsymbol{a}_1(\tau) \otimes \boldsymbol{a}_2(\theta)$ yields a 2D steering vector $\boldsymbol{a}(\theta, \tau)$. The parameter λ is the wavelength of the transmission signal, d is the received element interval, θ is the arrival angle, μ is the chirp rate of the radar, B_w is the transmission bandwidth, and T_m is the chirp signal duration. Also, Δt is the sampling interval, and τ is the delay time from when a transmission signal is radiated to when it is reflected by a target and returns to the receiving element. Since the delay time is equivalent to the information on the distance from the radar to an object, we scan the angle of $\boldsymbol{a}(\theta, \tau)$ and the delay time in the spectrum $\boldsymbol{P}_{2D-BF}(\theta, \tau)$ of the above equation to detect the peak in order to estimate the location of the target. Note that the 2D-MUSIC method can be explained in a similar manner.

We also review the 2D-BF-KR method, in which KR product extension is applied to the 2D-BF method. Until the correlation matrix $\boldsymbol{R}_{xx}$ is calculated, the procedure is the same as that of the 2D-BF method, so we omit these steps. A vectorization operation is performed on the correlation matrix $\boldsymbol{R}_{xx}$ to generate a KR-product-extended received signal:

$$\boldsymbol{z} = \mathrm{vec}(\boldsymbol{R}_{\mathrm{xx}}) = \boldsymbol{A}'\boldsymbol{s} + \boldsymbol{q}\mathrm{vec}(\boldsymbol{R}_N), \tag{12}$$

where $\boldsymbol{z}$ denotes a received signal extended by the KR product. The direction matrix $\boldsymbol{A}$ changes to a KR-product-extended steering matrix $\boldsymbol{A}'$ in $\boldsymbol{z}$, and the number of elements of

978-1-7281-2660-9/19/$31.00 ©2019 IEEE

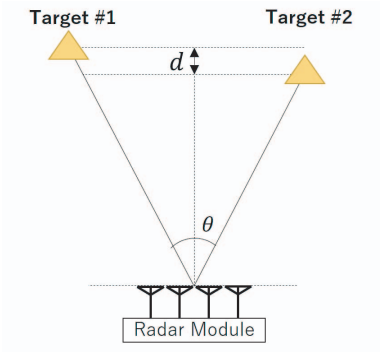

Fig. 1. FMCW-SIMO/MIMO radar system.

TABLE I
SPECIFICATIONS OF THE FMCW RADAR SYSTEM.

carrier frequency	79 GHz
bandwidth	3.16 GHz
SNR	10 dB (AWGN)
sampling frequency	5.5 MHz
# of time snapshots	256
# of transmitter antennas	1
# of receiver antennas	4
array configuration	ULA (in case without KR) nested array (in case with KR)
receiver antenna interval	half wavelength
# of chirp pulses	4

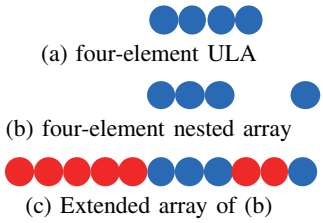

(a) four-element ULA

(b) four-element nested array

(c) Extended array of (b)

Fig. 2. Configurations of linear arrays, where blue and red circles mean physical (real) and virtual array elements.

the direction vector for each incoming wave increases. This process virtually increases the number of antenna elements and the number of sampling points. Next, a new correlation matrix $\boldsymbol{R}_{zz} = E[\boldsymbol{z}\boldsymbol{z}^H]$ is generated from the KR-product-extended received signal $\boldsymbol{z}$. By multiplying this correlation matrix by the steering vector $\boldsymbol{a}_{kr}(\theta,\tau)$, it is possible to calculate the distance and angle spectrum $\boldsymbol{P}_{2D-BF-KR}(\theta,\tau)$. The formula for calculating the spectrum is

$$\boldsymbol{P}_{2D-BF-KR}(\theta,\tau) = \frac{\boldsymbol{a}_{kr}^H(\theta,\tau)\boldsymbol{R}_{zz}\boldsymbol{a}_{kr}(\theta,\tau)}{\boldsymbol{a}_{kr}^H(\theta,\tau)\boldsymbol{a}_{kr}(\theta,\tau)}, \quad (13)$$

$$\boldsymbol{a}_{kr}(\theta,\tau) = \boldsymbol{a}'(\tau)\otimes\boldsymbol{a}'(\theta), \quad (14)$$

$$\boldsymbol{a}'(\theta) = \left[1, e^{j\frac{2\pi}{\lambda}d_1\sin\theta}, \cdots, e^{j\frac{2\pi}{\lambda}d_{2K-2}\sin\theta}\right]^T, \quad (15)$$

$$\boldsymbol{a}'(\tau) = \left[1, e^{j\mu\tau\Delta t}, \cdots, e^{j\mu(2N-2)\tau\Delta t}\right]^T, \quad (16)$$

where $\boldsymbol{a}'(\tau)$ and $\boldsymbol{a}'(\theta)$ are steering vectors extended by the KR product and have time and angle information, respectively. The Kronecker product of these vectors yields 2D steering vectors $\boldsymbol{a}_{kr}(\theta,\tau)$. Note that the 2D-MUSIC-KR method can be explained in a similar manner.

III. EVALUATION IN SIMULATION

We evaluated the accuracy of location estimation with the MM-wave FMCW-MIMO radar when KR product extension was applied to the receiver array antenna. Location estimation can be regarded as a combination of distance and DOA estimation, and the accuracy of distance estimation basically depends on the FFT resolution. Therefore, we focused on the accuracy in DOA estimation with the MM-wave FMCW-MIMO radar and on how the virtual array elements work.

A. Simulation specifications

We considered an FMCW-SIMO/MIMO radar system as shown in Fig. 1, with two targets (reflectors) in a far field from the radar module. The targets were located with the distance difference d and the angle difference θ as in Fig. 1. Table I shows the specifications of the FMCW radar system. We adopted the ULA configuration in Fig. 2(a) for the non-extended arrays and the nested array in Fig. 2(b) for the extended arrays. Note that the nested array in Fig. 2(b) can create virtual elements as in Fig. 2(c). We assumed omni-directional antenna element directivity and no mutual coupling effect in the simulation, and we evaluated the DOA estimation accuracy of waves reflected from targets.

We tested two cases, $d = 0$ and 3 cm, while changing the location of two targets so that the angle differences θ became $2, 4, 8, 12, 16, 20, 24, 28$ and 32 degrees. We first evaluated the minimum angle difference θ_0 at which two waves were successfully separated. We also evaluated the DOA estimation error by using the root mean square error (RMSE) between the true and estimated angles in the case of DOAs with angle difference θ_0.

The DOA estimation methods to be evaluated are as listed in Table II and Fig. 3, where the abbreviations "-KR" and "SSn" respectively mean the application of KR product extension and SSP extension, where n denotes the number of subarray elements. The specifications of the computer used in the simulation are as follows. The OS was Windows 10, the CPU was a 4.20 GHz, Intel Core i7-7700K, the memory was 8 GB , and the language was Python version 3.6.

B. Resolution of DOA estimation methods

Table II shows a comparison of the minimum angle difference θ_0 at which two waves were successfully separated with a probability of more than 95% and the DOA estimation error in terms of RMSE for the various DOA estimation methods in the cases of $d = 0$ and 3 cm. For 2D-MUSIC and 2D-MUSIC-KR [9], the number of sub-snapshots $N_s = 64$ was used to perform the averaging operation in the time domain. Also note that the RMSE was evaluated only when two waves were successfully separated. There was no difference in distance from the two targets in the case of $d = 0$ cm; therefore, the received signals became coherent. We expect that MUSIC-based methods will

978-1-7281-2660-9/19/$31.00 ©2019 IEEE

TABLE II
COMPARISON OF DOA ESTIMATION ACCURACIES.

Method	$d = 0$ cm		$d = 3$ cm	
	θ_0 [deg.]	RMSE [deg.]	θ_0 [deg.]	RMSE [deg.]
BF	32.0	5.91	32.0	3.16
BF-KR	16.0	5.65	16.0	5.65
BF-KR-SS5	16.0	7.07	16.0	6.40
BF-KR-SS6	16.0	7.07	16.0	6.40
MUSIC	-	-	12.0	1.10
MUSIC-SS3	24.0	0.68	16.0	0.65
MUSIC-KR-SS5	4.0	4.28	4.0	7.85
MUSIC-KR-SS6	4.0	4.25	4.0	7.66
2D-BF	28.0	3.50	16.0	5.68
2D-BF-KR	16.0	3.77	8.0	1.21
2D-MUSIC-SS3	20.0	1.31	4.0	1.40
2D-MUSIC-KR-SS5	2.0	1.95	8.0	1.05
2D-MUSIC-KR-SS6	2.0	2.24	2.0	0.50

not be good at estimating the DOAs of such signals without SSP or any other correlation suppression technique.

We see from Table II that the DOA estimation performance in the case of $d = 0$ cm became poor overall for the BF-based and MUSIC-based methods without SSP due to the high correlation between the two reflected waves. Also note that the standard MUSIC method could not separate the two waves at all in the case of $d = 0$ cm because of the coherency of the two waves. We also see from Table II that the methods with KR extension achieved very high separability, and the 2D-MUSIC-based methods [9] achieved a good DOA estimation accuracy.

Fig. 3 shows the quartile deviations of RMSE for the various angles of $\theta = 2, 4, 8, 12, 16, 20, 24, 28$ and 32 degrees. We see from Table II and Fig. 3 that the methods based on MUSIC and 2D-MUSIC had relatively higher resolutions than the BF-based methods, so we confirmed that KR extension worked effectively. However, we also see from Fig. 3 that the estimation error sometimes became large in the cases of large values of θ, even for the methods that can achieve a high resolution.

On the basis of these simulation results, we chose four methods, BF-KR, 2D-BF-KR, MUSIC-KR-SS6, and 2D-MUSIC-KR-SS6, that often had relatively good resolutions and high rates of successful estimation. We evaluated these four methods in experiments in the next section.

C. Snapshot dependency of methods with KR extension

We also studied the snapshot dependency of the RMSEs of the methods with KR extension, i.e., the behavior of RMSE for various values of snapshots. The DOA estimation error generally came to be in inverse proportion to the number of snapshots; however, we found that it became almost periodic for the methods with KR extension.

Fig. 4 shows the behavior of the RMSE for the MUSIC methods with and without KR extension for various values of snapshots. We see from Fig. 4 that the behavior of the RMSE for the method with KR extension became almost periodic against the number of snapshots. This is because

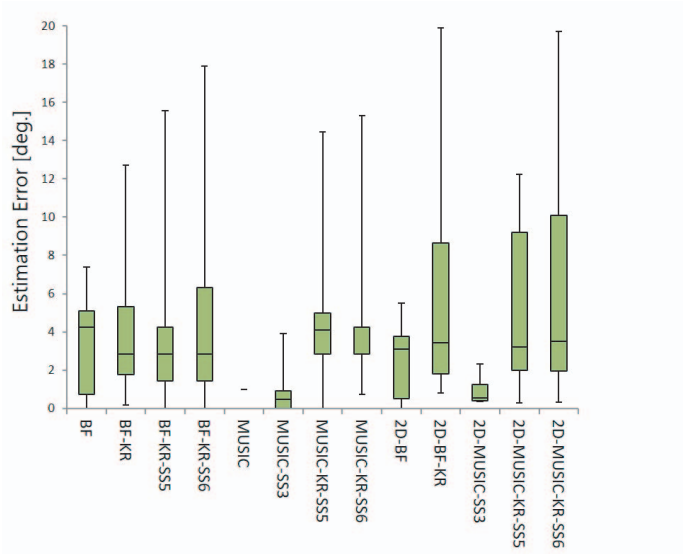

(a) in case of $d = 0$ cm

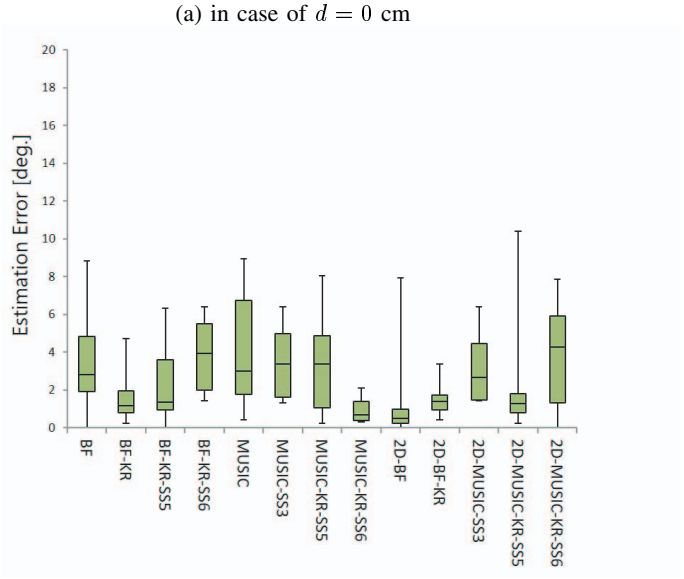

(b) in case of $d = 3$ cm

Fig. 3. Quartile deviations of DOA estimation errors.

KR extension works only when signals are quasi-stationary; indeed, the RMSE becomes small when the signals are regarded as stationary but becomes large when the signals cannot be regarded as stationary. The period will be dependent on the DOA as seen in the comparison of Figs. 4(a) and 4(b). However, we did not have any prior information on the DOAs and therefore had no idea how to determine the appropriate number of snapshots prior to DOA estimation.

IV. EVALUATION IN EXPERIMENTS

We also evaluated the accuracy of location estimation through experiments using a real FMCW-MIMO radar system.

A. Experimental set-up

Here, we evaluate the performance of a 2×4 FMCW-MIMO radar system (with two transmitters and four receiver

978-1-7281-2660-9/19/$31.00 ©2019 IEEE

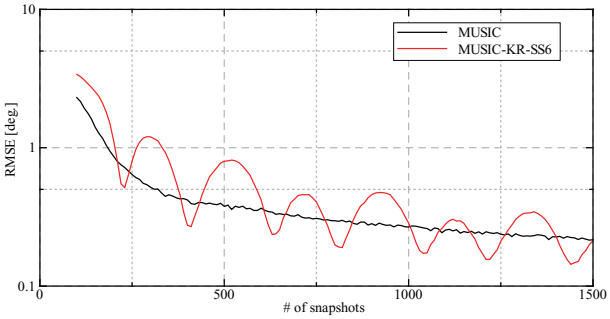

(a) in case of $d = 3$ cm

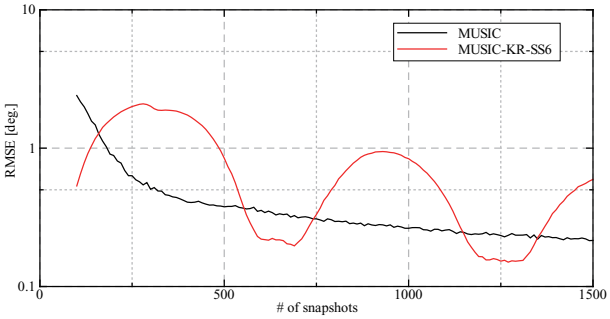

(b) in case of $d = 2$ cm

Fig. 4. Behavior of RMSE for various values of snapshots in case of DOAs of -15 and 15 degrees and SNR of 0 dB.

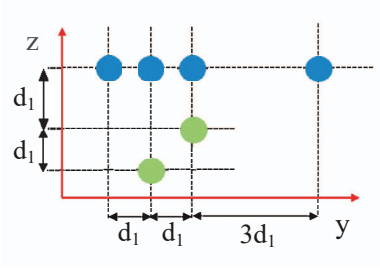

Fig. 5. Configuration of MIMO antennas, where green and blue circles respectively denote transmitter and receiver elements.

antenna elements) by using actual measurement data obtained in an anechoic chamber. Fig. 5 shows the configuration of the MIMO transmitter/receiver antenna elements used in the experiments. The configuration of the receiver elements in Fig. 5 was a four-element nested array [14], where the element interval d_1 is the half wavelength of the carrier frequency. Note that the 2×4 FMCW-MIMO radar system is equivalent to an SIMO radar with eight-element array (blue circles in Fig. 6) in DOA estimation. Furthermore, by applying KR product extension to the received signal of this MIMO-extended antenna array, it is virtually extended up to 33 elements as shown in Fig. 6. The specifications of this experiment basically followed those of the simulation in Table I, and the experiments were performed in the anechoic chamber shown in Fig. 7.

B. Result of experiments

Similarly to Table II, we evaluated the minimum separable angle θ_0 in the cases of $d = 0$ and 3 cm for four methods, BF-KR, 2D-BF-KR, MUSIC-KR-SS6, and 2D-MUSIC-KR-SS6, through our experiments. Table III shows the observed values of θ_0 in each case. We made the following observations as shown in Table III. First, the MUSIC-based methods had a better estimation accuracy overall. Second, BF-KR and MUSIC-KR-SS6 could not improve the separation performance even in the case of $d = 3$ cm. Last, 2D-BF-KR and 2D-MUSIC-KR-SS6 achieved a much smaller angle θ_0 in the case of $d = 3$ cm, meaning that these methods were not good at estimating the DOAs of coherent signals but were good at doing so for lowly correlated signals ($d = 3$ cm).

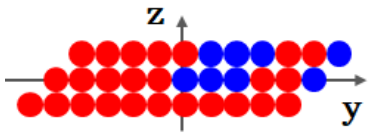

Fig. 6. Configuration of extended array corresponding to Fig. 2, where blue and red circles respectively denote physical (real) and virtual elements.

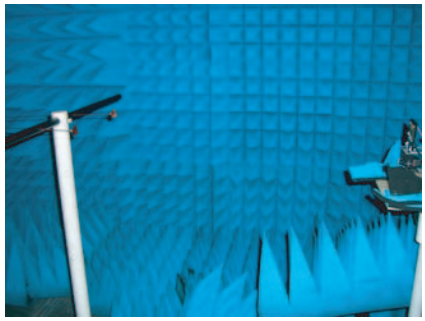

Fig. 7. Experiments in anechoic chamber with MIMO radar (right) and reflectors (left, at edges of horizontal pole).

Also, Fig. 8 shows the behavior of RMSE in case of close-angle waves. We see from Fig. 8 that all four of the methods well estimated DOAs overall. In particular, the methods with KR extension often produced small estimation errors; however, the error suddenly became large in the case of $d = 3$ cm and $\theta = 16$ degrees. This would be because of the non-stationary characteristics of incident signals as we discussed in subsection III-C, which may have caused such a large error.

The estimators worked well overall. We also show spectral (heat) map for the well-estimated case in Fig. 9 in the case of $d = 3$ cm. We can see from Fig. 9 that 2D-MUSIC-KR-SS6 clearly detected the two targets, while 2D-BF-KR could not separate the two targets. We confirmed the superiority of target separability and DOA estimation accuracy as shown Table III and Fig. 9.

V. Conclusion

In this paper, we evaluated the performance of location estimation with various estimation methods for the MM-wave FMCW-MIMO radar. We observed that KR extension often worked effectively, and it successfully estimated DOAs with a high resolution and high accuracy. However, we found

978-1-7281-2660-9/19/$31.00 ©2019 IEEE

TABLE III
COMPARISON OF MINIMUM SEPARABLE ANGLES [DEG.].

Methods	$d = 0$ cm	$d = 3$ cm
BF-KR	16.0	16.0
2D-BF-KR	12.0	4.1
MUSIC-KR-SS6	4.0	8.1
2D-MUSIC-KR-SS6	12.0	4.1

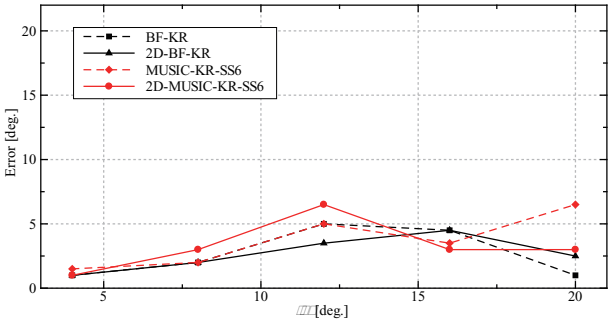

(a) in case of $d = 0$ cm

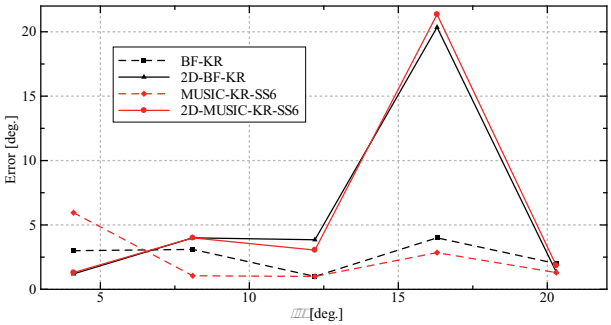

(b) in case of $d = 3$ cm

Fig. 8. Behavior of RMSE in case of close-angle waves.

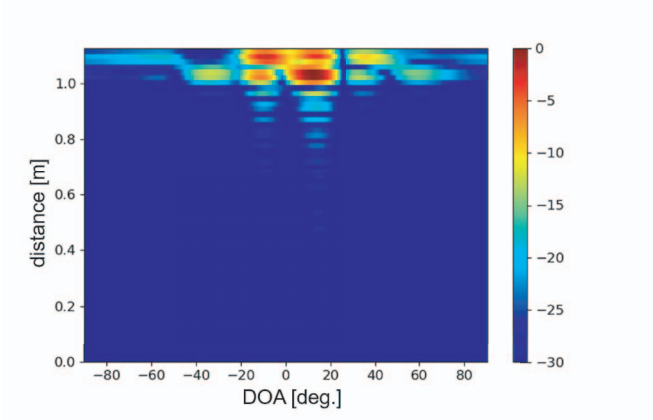

(a) with 2D-BF-KR

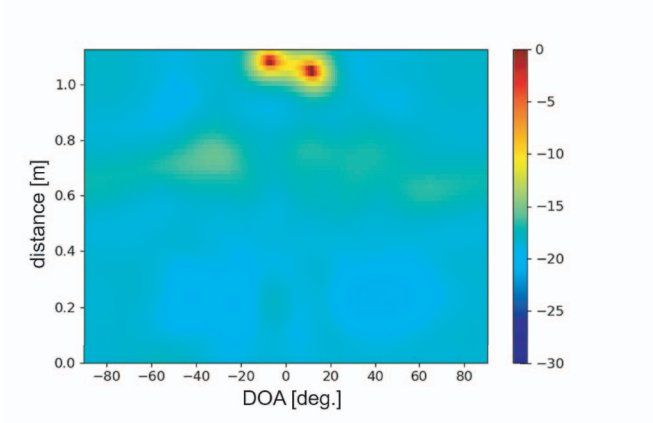

(b) with 2D-MUSIC-KR-SS6

Fig. 9. Spectral (heat) maps in case of successful estimation.

that KR product extension was not versatile, was not always good at separating close-angle waves, and sometimes failed to estimate the DOAs of the incident waves with a particular angle distance.

VI. ACKNOWLEDGMENTS

This work was supported in part by the Support Center for Advanced Telecommunications Technology Research Foundation (SCAT). The authors are sincerely grateful for the support.

REFERENCES

[1] K. Bimbraw, "Autonomous Cars: Past, Present and Future - A Review of the Developments in the Last Century, the Present Scenario and the Expected Future of Autonomous Vehicle Technology," Proc. International Conference on Informatics in Control, Automation and Robotics (ICINCO), Colmar, pp. 191–198, 2015.

[2] Texas Instruments, Advanced Driver Assistance Systems (ADAS), http://www.ti.com/applications/automotive/adas/overview.html

[3] Texas Instruments, Automotive mmWave sensors, http://www.ti.com/sensors/mmwave/awr/overview.html

[4] S. Patole, M. Torlak, D. Wang, and M. Ali, "Automotive Radars: A Review of Signal Processing Techniques," IEEE Signal Processing Magazine, vol. 34, no. 2, pp. 22–35, Mar. 2017.

[5] D. G. Oh and J. H. Lee, "Low-Complexity Range-Azimuth FMCW Radar Sensor Using Joint Angle and Delay Estimation Without SVD and EVD," IEEE Sensors Journal, vol. 15, no. 9, pp. 4799–4811, Sept. 2015.

[6] S. Theodoridis and R. Chellappa, Academic Press Library in Signal Processing, Volume 3: Array and Statistical Signal Processing, Academic Press, 2013.

[7] S. Kim, D. G. Oh, and J. H. Lee, "Joint DFT-ESPRIT Estimation for TOA and DOA in Vehicle FMCW Radars," IEEE Antennas and Wireless Propagation Letters, vol. 14, pp. 1710–1713, Apr. 2015.

[8] D. G. Oh, Y. H. Ju, and J. H. Lee, "Subspace-Based Auto-Paired Range and DOA Estimation of Dual-Channel FMCW Radar without Joint Diagonalization," Electronics Letters, vol. 50, no. 18, pp. 1320–1322, Aug. 2014.

[9] Y. Wakamatsu, H. Yamada, and Y. Yamaguchi, "MIMO Doppler Radar Using Khatri-Rao Product Virtual Array for Indoor Human Detection," IEICE Transactions on Communications, vol. E99-B, no. 1, pp. 124–133, Jan. 2016.

[10] R. O. Schmidt, "Multiple Emitter Location and Signal Parameter Estimation," IEEE Trans. Antennas and Propagation, vol. 34, pp. 276–280, Mar. 1986.

[11] R. Roy and T. Kailath, "ESPRIT-estimation of Signal Parameters via Rotational Invariance Techniques," IEEE Trans. Acoust., Speech and Signal Processing, vol. 37, no. 7, pp. 984–995, July 1989.

[12] T. J. Shan, M. Wax, and T. Kailath, "On Spatial Smoothing for Direction-of-Arrival Estimation of Coherent Signals," IEEE Trans. Acoust., Speech, Signal Process., vol. 33, no. 4, pp. 806–811, Aug. 1985.

[13] W. K. Ma, T. H. Hsieh, and C. Y. Chi, "DOA Estimation of Quasi-Stationary Signals via Khatri-Rao Subspace," IEEE Proc. Int. Conf. Acoustic. Speech Signal Process., pp. 2165–2168, Apr. 2009.

[14] P. Pal and P. P. Vaidyanathan, "Nested Arrays: A Novel Approach to Array Processing With Enhanced Degrees of Freedom," IEEE Trans. Signal Processing, vol. 58, no. 8, pp. 4167–4181, Aug. 2010.

978-1-7281-2660-9/19/$31.00 ©2019 IEEE